Analytical and Numerical Study on the Pillar Rockbursts Mechanism

By

S. Y. Wang[1]**, K. C. Lam**[1]**, S. K. Au**[1]**, C. A. Tang**[2]**,
W. C. Zhu**[2]**, and T. H. Yang**[2]

[1] Department of Building and Construction, City University of Hong Kong,
Kowloon, Hong Kong
[2] Center for Rock Instability and Seismicity Research, Northeastern University,
Shenyang, P.R. China

Summary

Based on cusp-type catastrophe theory, a sample rock–rock model for studying the pillar rockburst mechanism is presented in this paper. It is shown that the stiffness ratio, K, of the roof and floor to the pillar plays an important role in the outbreak of instability. Additionally, simple formulae for the deformation jump and the energy release are derived. Based on the assumption that there exists a proportional relationship between the number of microseismic events and microfractured elements, the theoretical microseismic event rate produced by the double rock sample, loaded in series under uniaxial compression, is obtained. Using a newly developed numerical code, RFPA^{2D}, the progressive failure process and associated microseismic behavior of the twin rock samples are simulated, which shows that the spatial distribution of microseismic events develops progressively from disorder at the initial loading stage to order prior to the main shock. The numerically simulated results also confirm that a soft roof and floor promote an unstable failure or collapse of pillars, while a stiff roof and floor can lead to a stable failure of pillars. Additionally, the simulated results reproduce the deformation jump and the energy release that occur during a pillar rockburst. It is demonstrated that the proposed model properly simulates the pillar failure process.

Keywords: Cusp type catastrophe theory, numerical simulation, rockburst.

1. Introduction

Rockbursts are sudden, explosion-like events that occur deep underground, posing a hazard to the safety of underground miners and causing damage to mine structures. Rock-bursts inside any mining excavation are essentially rock failures due to alteration of the virgin state of stress. Such alteration results directly from mining and

creating an opening through the rock mass. As mining depth increases, the influence of seismic effects in a mine becomes more critical due to the progressive increase in ambient stresses. Being a seismic event, a rock-burst usually results in damage to underground workings. This is due to the uncontrolled disruption of the rock equilibrium and the release of the strain energy stored in the rock body (Cook, 1976).

Rockbursts represent only a small subset of the large set of seismic events that occur in seismically-active mines. The following statement was made by Salamon in 1993: ''Virtually no systematic research has been done to elucidate the basis of setting apart those seismic events which become rockbursts from those which do not.'' To make progress in understanding the process of rockbursts, it is essential to create a tool which provides the opportunity to relate seismicity to induced disturbances.

In the late 1950s and early 1960s, researchers proposed a simple analogy between the violent failure of a rock sample in a soft-testing machine and the dynamic rock fracture that occurs during rockbursts (Gill et al., 1993). With this analogy, the rock specimen, being in a uniaxial compressive state of stress, acts as the fractured rock and the loading system acts as the surrounding rock mass. In this way, a stiffness criterion for instability can be obtained. If the post-peak stiffness of the rock specimen is less than the load system stiffness, the equilibrium state becomes unstable and the failure of the rock specimen is violent. Otherwise, the equilibrium state becomes stable and failure occurs gradually. In most cases presented in the past, the system discussed were composed of a rock specimen and a soft-testing machine. However, some problems arise with this approach (Tang et al., 1993). The first is that the surrounding rock mass could be an inelastic body instead of an elastic body like the soft-testing machine. The second is that no micro-seismic events can be produced in the loading machine in the process of rock specimen failure. For the surrounding rock mass, however, some microseismic events might be produced during the loading process. The third is that the changes in seismic activity occurring in the unstable failure of rock are mainly concentrated in the failed body of the rock mass and less attention is paid to the surrounding rock mass which, in fact, could involve forewarning signs of seismic activity prior to the unstable failure associated with rockbursts.

During recent decades, extensive research has been focused on the mechanisms of rockbursts and how to predict their occurrence. The various attempts have included: the micro-gravity method, the rebound method, the drilling-yield method, and the microseismic method. However, few approaches have been found to be particularly successful. The reason for this may be: (1) that the precise physical mechanism of rockburst is very complicated and, therefore, it is difficult to establish a simple mechanical model for rockburst; and (2) that the seismic data monitored in situ are not completely or appropriately utilized.

It is well known that rockbursts are discontinuity phenomena that behave dramatically. Therefore, it is very difficult to study them using traditional mathematical techniques that focus on continuous behaviour. Catastrophe Theory, which is a part of mathematics, is a theory about singularities that deals with the properties of discontinuities directly. It was developed by the French mathematician Thom (Saunders, 1980). Many discontinuous phenomena, such as slope instability, reservoir-induced earthquakes, coal pillar bursting, rock specimen instability and fault movement, which

have been mathematically intractable before, can be dealt with using Catastrophe Theory (Henley, 1976; Cubiu and Shaw, 1976; Rice, 1983; Yin and Zheng, 1988). Most rock pillar failures can be regarded as discontinuous, catastrophic phenomena. Therefore, it is appropriate to use catastrophe theory to study rock pillar failure.

In the first part of this paper, based on cusp-type catastrophic theory, a double rock sample model for studying the pillar rockburst mechanism is introduced. This is invoked to enhance understanding of rockburst mechanisms, e.g. how a rockburst occurs in terms of the interaction between the failed rock mass and the surrounding rock mass. In the second part, the progressive failure process and associated seismicity in rock samples is simulated with a newly developed numerical code, RFPA^{2D}. Specifically studied is the influence of the relative stiffness between roof and floor on pillar failure under a uniform vertical displacement boundary. In addition, the sudden stress drop and deformation jump that occur during the process of unstable pillar failure is examined. Agreement is then sought between the observed phenomena and the cusp-type catastrophe model, which addresses the properties of discontinuities directly.

2. Theoretical Considerations

2.1 A Brief Introduction to Catastrophe Theory

As described by Saunders (1980), a system whose behaviour is usually smooth but sometimes (or in some places) exhibits discontinuities is considered here. It is supposed that without much loss the state of the system at any time can be completely specified by supplying the values of n variables $(x_1, x_2 \ldots x_n)$, and that the system is under the control of m independent variables $(p_1, p_2 \ldots p_m)$, with the values of these variables determining those of the x_i. The x_i are referred to as state variables and the p_i as control variables.

Based on an understanding of Catastrophe Theory, the number of qualitatively different configurations of discontinuities that can occur depends not only on the number of state variables, which may be very large, but also on the number of control variables. In particular, if the number of control variables is not greater than four, then there are only seven distinct types of catastrophes, and in none of these are more than two state variables involved. One of them, called a cusp catastrophe, has two control variables and one state variable, and will be used in this paper. Its standard form of potential $V(x)$ is as follows:

$$V(x) = \frac{1}{4}x^4 + \frac{p}{2}x^2 + qx, \qquad (2.1)$$

where x is the state variable and p, q are the control variables. The phase space is thus three-dimensional. It is defined that the equilibrium surface, M, is given by the equation

$$\nabla_x V = 0, \qquad (2.2)$$

where the subscript x indicates that the gradient is with respect to the state variable only. This surface is made up of all the critical points of V, i.e., all the equilibria (stable or otherwise) of the system. M is denoted to indicate that it is a manifold, that is a

well-behaved smooth surface. For the cusp catastrophe, the equilibrium surface M is given by

$$\nabla_x V = x^3 + px + q = 0. \tag{2.3}$$

Next it is easy to find the singularity set, S, which is the subset of M that consists of all the degenerate critical points of V. These are the points at which $\nabla_x V = 0$ and also

$$\Delta \equiv \det\{H(V)\} = 0, \tag{2.4}$$

where $H(V)$ is called the Hessian of V, the matrix of second order partial derivatives as follows:

$$\begin{bmatrix} \dfrac{\partial^2 V}{\partial x_1^2} & \dfrac{\partial^2 V}{\partial x_1 \partial x_2} & \cdots & \dfrac{\partial^2 V}{\partial x_1 \partial x_n} \\ \dfrac{\partial^2 V}{\partial x_2 \partial x_1} & \dfrac{\partial^2 V}{\partial x_2^2} & \cdots & \dfrac{\partial^2 V}{\partial x_2 \partial x_n} \\ \cdots & \cdots & \cdots & \cdots \\ \dfrac{\partial^2 V}{\partial x_n \partial x_1} & \dfrac{\partial^2 V}{\partial x_n \partial x_2} & \cdots & \dfrac{\partial^2 V}{\partial x_n^2} \end{bmatrix},$$

where x_i are state variables. This gives

$$\nabla_x^2 V = 3x^2 + p = 0. \tag{2.5}$$

Then S is projected down into the control space C (by eliminating the state variables from the equations that define it) to obtain the bifurcation set, B, which is
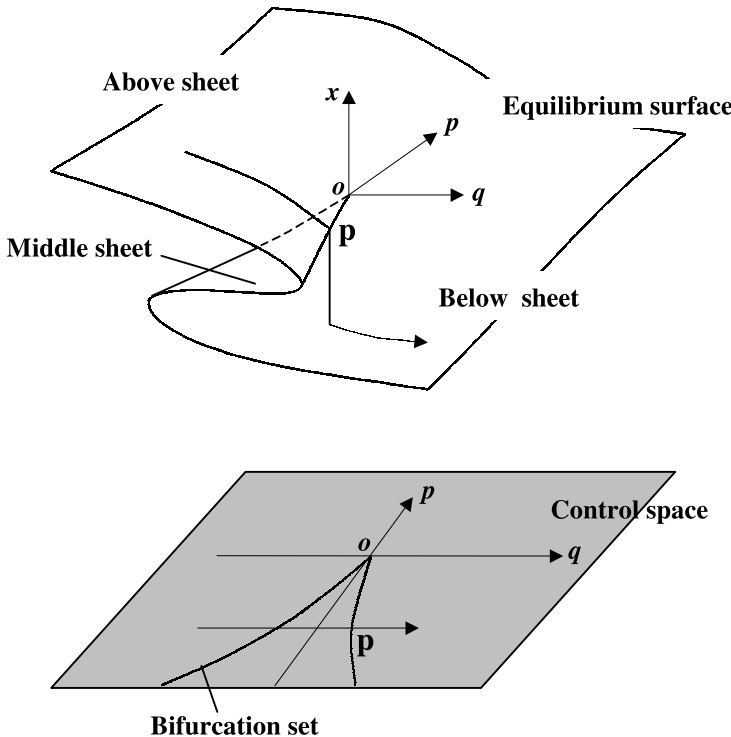

Fig. 1. The equilibrium surface and bifurcation set of the cusp catastrophe

the set of all points in C at which changes occur in the form of V. So by eliminating x from (2.3) and (2.5), we obtain the bifurcation set

$$4p^3 + 27q^2 = 0. \tag{2.6}$$

Finally, the form of V is determined at every point in C; this is easier than it sounds because changes can occur only on B and it is sufficient to consider only one point within each of the regions into which B divides C. It is easier to predict what will occur for different paths in the neighborhood of B if the surface is sketched as in Fig. 1. This is the set of equilibrium values of (x, p, q) for the cusp catastrophe (described by Eq. (2.3)). Considering the state of the system as being represented by a point P in three-dimensional phase space with x, p, q as coordinates, the phase point P must always lie on the surface. In fact it must lie on either the top or the bottom sheet, because the middle sheet corresponds to unstable equilibria.

The diagram can be interpreted as follows. The location of the point P is represented by a point in the p–q plane, which is called the control space. As the control variables p and q are altered, this control point traces out a path which is called the control trajectory. At the same time, the phase point moves along a trajectory in the equilibrium surface, directly above the control trajectory. Smooth variations in p and q almost always produce smooth variations in x. The only exceptions occur when the control trajectory crosses the bifurcation set B (described by Eq. (2.6)), which is the projection onto the p–q plane of the folds of the equilibrium surface. If the phase point happens to be on the surface that ends at this point then it must jump to the other sheet. This brings about a sudden change in x.

2.2 A Mechanics Model of the Rock–Rock (Hypocenter-Surrounding) System

A sketch of a rock–rock (hypocenter-surrounding) system is shown in Fig. 2, in which the rock in the hypocenter area and the rock in the surrounding area are substituted by
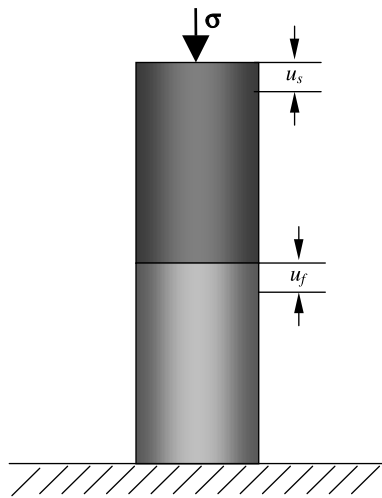
Fig. 2. Rock–rock (hypocenter-surrounding rock) sample model

an equivalent specimen-spring system interacting in series. The word "spring" is used for the surrounding rocks because they are assumed to be elastic and to have higher strength than the hypocenter. The instability behaviour of this system, which will be discussed here invoking Catastrophe Theory, throws new light on problems that are important to studies of instability.

During deformation, both the rock in the hypocenter area and the rock in the surrounding area are subjected to the same tectonic movement. In the simplest case, and if the process of deformation is viewed quasi-statically, the system is in equilibrium, that is

$$R_f = R_s, \tag{2.7}$$

where R_f is the load carrying capacity of rock in the hypocenter area (subscript f means the rock in the failure area; in the fault model, f also expresses "fault"), and R_s is the force acting on the spring, that is, the surrounding rocks (so here, subscript s means both "spring" and "surrounding"). The force acting on the spring is given by (in the elastic range)

$$R_s = f_s(u_s) = k_s u_s, \tag{2.8}$$

where k_s is the stiffness of the surrounding rock and u_s is its deformation.

The force-deformation relationship of the rock in the hypocenter area is non-linear. It can be seen that the feature of rock softening (weakening) is a prerequisite for system instability. Therefore, it is key to the study of rock instability to establish a constitutive law for rock that conforms to the actual reality of rock failure. The force-deformation relationship has been given by the equation (Tang, 1993)

$$\sigma = E\varepsilon \cdot e^{-\left(\frac{\varepsilon}{\varepsilon_0}\right)^m},$$

where m is the shape parameter, defined as the homogeneity index of the rock. For simplicity, let $m = 1$ in this equation, that is,

$$\sigma(\varepsilon) = E\varepsilon e^{-\frac{\varepsilon}{\varepsilon_0}}, \tag{2.9}$$

where E and ε_0 are coefficients determined by experiment.

For a hypocenter area with cross-sectional area A, and length L, Eq. (2.9) can be expressed in terms of R_f, the loading carrying capacity of the rock, and u_f, the rock deformation, in the following form:

$$R_f = f_f(u_f) = k_f u_f e^{-\frac{u_f}{u_0}}, \tag{2.10}$$

where $k_f = \frac{EA}{L}$ is the initial stiffness of specimen and u_0 is the value of deformation corresponding to the maximum load carrying capacity. For this Eq. (2.10), there exists an inflection in the curve at the point $u_f^* = 2u_0$, the absolute value of its slope being $k_f^* = k_f e^{-2}$.

2.3 Application of Catastrophe Theory

The most important step is to construct the potential function V of the system. The variable u_f (deformation of rock in the hypocenter area) can be used as the state

variable of the system. It is easy to see from Fig. 2 that the whole energy of the system can be expressed as follows:

$$V = (E_e^s + E_e^f) + E_c^f, \tag{2.11}$$

where E_e^s is the elastic energy stored in the surrounding rocks, E_e^f is the elastic energy stored in the hypocenter region, and E_c^f is the energy consumed in the failure of the rock. Thus, the following equation can be obtained:

$$V = (E_e^s + E_e^f) + E_c^f = \int_0^{u_f} f_f(z)dz + \int_0^{u_0} f_s(z)dz$$

$$= k_f u_0 \left[u_0 - (u_0 + u_f)e^{-\frac{u_f}{u_0}} \right] + \frac{1}{2}k_s u_s^2. \tag{2.12}$$

Considering $u_s = u_\infty - u_f$ (u_∞ is the so-called far-field displacement), the potential function of the system can be obtained by rewriting Eq. (2.12) as follows:

$$V = k_f u_0 \left[u_0 - (u_0 + u_f)e^{-\frac{u_f}{u_0}} \right] + \frac{1}{2}k_s(u_\infty - u_f)^2. \tag{2.13}$$

The equilibrium surface M is given by

$$\nabla_x V = k_f u_f e^{-\frac{u_f}{u_0}} - k_s(u_\infty - u_f) = 0. \tag{2.14}$$

It is easy to see that the above equation is simply the equilibrium Eq. (2.7). The singularity set is

$$\nabla_x^2 V = k_f \left(1 - \frac{u_f}{u_0} \right) e^{-\frac{M_f}{M_0}} + k_s = 0. \tag{2.15}$$

It is easy to find that Eq. (2.15) is irrelevant to the far-field displacement u_∞, but is relevant to the material parameter k_s, k_f, u_0 and the state variable u_f. That is to say the singularity set in which the catastrophe may occur is determined only by the characteristics of the mechanical system.

Now the cusp point can be obtained from

$$\nabla_x^3 V = \frac{k_f}{u_0} \left(\frac{u_f}{u_0} - 2 \right) e^{-\frac{u_f}{u_0}} = 0. \tag{2.16}$$

The solution of this equation is

$$u_f = u_f^* = 2u_0, \tag{2.17}$$

which is the inflection point of the force-deformation curve.

In order to obtain the standard format of the cusp model, the Taylor series expansion of Eq. (2.14) in $u_f = u_f^*$ is used and the terms are taken up to the third-degree. The following equation can be obtained.

$$k_f u_f^* e^{-\frac{u_f^*}{u_0}} - k_s(u_\infty - u_f^*) + \left[k_f \left(1 - \frac{u_f^*}{u_0} \right) e^{-\frac{u_f^*}{u_0}} + k_s \right](u_f - u_f^*)$$

$$+ \left[\frac{k_f}{2u_0} \left(\frac{u_f^*}{u_0} - 2 \right) e^{-\frac{u_f^*}{u_0}} \right](u_f - u_f^*)^2 + \left[\frac{k_f}{6u_0^2} \left(3 - \frac{u_f^*}{u_0} \right) e^{-\frac{u_f^*}{u_0}} \right](u_f - u_f^*)^3 = 0. \tag{2.18}$$

Since $u_f^* = 2u_0$, Eq. (5.18) can be simplified as

$$\frac{3}{2}\left[1 - \frac{k_s}{k_f e^{-2}}\left(\frac{u_\infty - u_f^*}{u_f^*}\right)\right] + \frac{3}{2}\left(\frac{k_s}{k_f e^{-2}} - 1\right)\left(\frac{u_f - u_f^*}{u_f^*}\right)^2 + \left(\frac{u_f - u_f^*}{u_f^*}\right)^3 = 0, \quad (2.19)$$

$$x^3 + px + q = 0. \quad (2.20)$$

This is the standard format of the cusp catastrophe model of the rock-specimen system where x is the dimensionless state variable

$$x = \frac{u_f - u_f^*}{u_f^*} \quad (2.21)$$

and

$$p = \frac{3}{2}(K - 1) \quad (2.22)$$

$$q = \frac{3}{2}(1 - K\xi) \quad (2.23)$$

$$K = \frac{k_s}{k_f e^{-2}} = \frac{k_s}{k_f^*} \quad (2.24)$$

$$\xi = \frac{u_\infty - u_f^*}{u_f^*}. \quad (2.25)$$

The parameter K is the stiffness ratio of the surrounding rock's stiffness k_s to the slope k_f^* at the inflection point of the rock force-deformation curve. Parameter ξ, which is a dimensionless parameter correlated to far-field displacement u_∞, is called the far-field displacement parameter (also called disturbance). From Eqs. (2.22) and (2.23), it can be seen that the control variables p and q are governed by the stiffness K and the far field displacement parameter ξ.

The relation between the state variable x and the control variables p and q is described by Eq. (2.20). The bifurcation set is determined by Eq. (2.6), which is a half parabolic curve and having its cusp at the coordinates (0,0). The control space is divided into two parts by the bifurcation set. In the small area, there exist three equilibrium points of which two are stable and one is unstable. In the large area, only one stable equilibrium point exists. In the bifurcation set, there are two-equilibrium states, one being stable and the other is unstable. If the control variables (p, q) vary smoothly in the control space, the number of equilibrium points (or point) and the stability of the system will not change unless (p, q) crosses the bifurcation set. If they do, it will cause a sudden change in state variable x.

2.4 Criterion for Instability

Because Eq. (2.6) is satisfied only when $p \leq 0$ (it is easy to see this from Fig. 1), the necessary condition for the system to reach its catastrophe state is

$$K - 1 \leq 0. \quad (2.26)$$

From Eq. (2.23) we have

$$k_s - k_f^* \leq 0, \qquad (2.27)$$

or

$$k_s + f_f'(u_f^*) \leq 0. \qquad (2.28)$$

That is to say, the necessary unstable condition is determined completely by the internal characteristics of the system itself. For instance, the material properties play an important role in the system behaviour besides geometric properties. If the rock is strain hardening or ideally plastic in character then, from Eqs. (2.27) and (2.28), the system must be stable. The instability will occur only when the rock has a softening characteristic.

From Eq. (2.23), it can be seen that the control variable q will decrease when the far-field displacement parameter ξ increases. The value of ξ when the bifurcation set is crossed can be determined now by inserting Eqs. (2.22) and (2.23) into Eq. (2.26) as follows:

$$\xi = \frac{1}{K}\left[1 \pm \frac{\sqrt{3}}{3}(1-K)^{\frac{3}{2}}\right]. \qquad (2.29)$$

So for every value of K, there exist two values of ξ. The small value corresponds to the right side of the bifurcation set ($q > 0$), in which state the so-called catastrophe only causes a sudden change of the mathematical structure (the number of equilibrium states and the stability), but do not cause any sudden jump in the state variable x. Therefore, we are more interested in the state when the left side of the bifurcation set ($q < 0$) is crossed, in which case the state of the system is unstable and a sudden jump in the state variable x occurs.

2.5 Sudden Jumps in Rock Deformation or Rock Deformation and Stress Drop

Now, it is time to determine the value of x corresponding to the control variables p, q on the left side of the bifurcation set. In the case when Eq. (2.6) is satisfied, Eq. (2.20) has a triple root $x_1 = x_2 = x_3 = 0$ when $p = 0$ and has three distinct real roots when $p < 0$ as follows:

$$x_1 = 2\left(\frac{-p}{3}\right)^{\frac{1}{2}} = \sqrt{2}(1-K)^{\frac{1}{2}}, \qquad (2.30)$$

$$x_1 = x_3 = -\left(\frac{-p}{3}\right)^{\frac{1}{2}} = -\frac{\sqrt{2}}{2}(1-K)^{\frac{1}{2}}. \qquad (2.31)$$

Thus a sudden jump in the state variable when the control variables cross the bifurcation set can be calculated as follows (and as shown in Fig. 3):

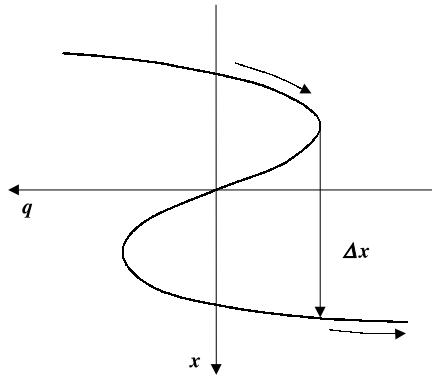$$\Delta x = x_1 - x_2 = \frac{3\sqrt{2}}{2}(1-K)^{\frac{1}{2}}. \qquad (2.32)$$

Fig. 3. The state jump that occurs when crossing the bifurcation set
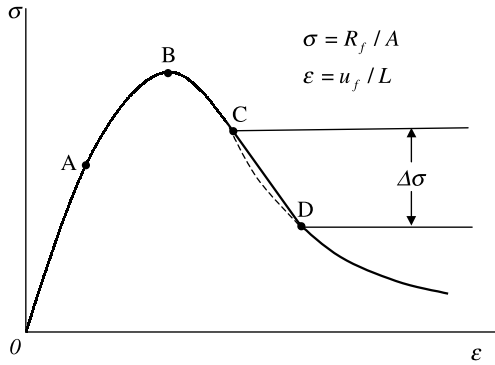

Fig. 4. Rock deformation jump

The corresponding rock deformation jump in the unstable state is

$$\Delta u_f = u_{f1} - u_{f2} = u_f^* \cdot \Delta x = 3\sqrt{2}u_0(1-K)^{\frac{1}{2}} = 3\sqrt{2}u_0\left(1 - \frac{k_s}{k_f^*}\right)^{\frac{1}{2}}. \qquad (2.33)$$

This is independent of the far-field displacement u_∞ and is only relevant to the intrinsic properties of the system.

This deformation jump is shown in Fig. 4, expressed by points C and D. Points C and D are the unstable equilibrium and stable equilibrium points, respectively. The process of rock failure instability usually does not extend to complete rock failure, but rather will slow down at point D, that is, from the unstable state C to the stable state D. This is compatible with natural phenomena, e.g. earthquakes (just because an earthquake occurs in a region does not mean that the whole rock mass in this region will fail completely and immediately).

The whole process of deformation can be divided into four stages:

1) From A to B (maximum strength). The deformation increases gradually;
2) From B to C. The deformation will obviously accelerate in this stage;

3) From C to D. A sudden jump occurs;

4) The unstable failure is terminated at D, and then returns to the normal state, i.e., stable state.

The energy difference between the pre-jump and the post-jump states is

$$\Delta U = U(x_1) - U(x_2) = x_1^4 - x_2^4 + 2p(x_1^2 - x_2^2) + 4q(x_1 - x_2). \tag{2.38}$$

Substituting Eqs. (2.30) and (2.31) for x_1 and x_2 and jointly using Eq. (2.22), one has

$$\Delta U = \frac{1}{3}p^2 = \frac{3}{4}(1 - K)^2. \tag{2.39}$$

Thus, the released energy is

$$\Delta U = \frac{1}{2}k_f^* u_0^2 (1 - K)^2. \tag{2.40}$$

Again, it can be seen that the energy released in the jump is independent of the far-field displacement u_∞ and is only related to the intrinsic properties of the system, such as the stiffness ratio, the geometrical properties and the material parameters. The energy released in the jump will increase when the stiffness ratio K decreases. When $K \to 0$, the released energy becomes a maximum:

$$\Delta V_{\max} = \frac{1}{2}k_f^* u_0^2. \tag{2.41}$$

3. Numerical Simulation

There are two deficiencies in the theoretical considerations. One is that the interaction among the elements has not been considered; the other is that the spatial distribution of the microseismic events cannot be obtained. Numerical simulations may remedy these deficiencies (Lockner and Madden, 1991; Lockner et al., 1992; Krajcinovic and Sumarac, 1989).

In the numerical analyses provided here, the theory of elasticity was used to estimate the stresses, and some strength criteria were applied to describe the rock failure under axial loading. The rock failure process is actually the accumulation, clustering and coalescence of microfractures, while the progressive development of fracture damage accounts greatly for the formation of cracks. Therefore the mechanisms of rock breakage can be explored more deeply with the inclusion of damage development. A statistical damage model seems to provide a good description of progressive fracture development. The combination of statistical theory and numerical models was found to be appropriate for modelling the progressive damage process for brittle materials such as rock.

As we know, rock is a heterogeneous material. Statistically, it is assumed that the local mechanical parameters are distributed following a certain probability distribution, based on previous work (Weibull, 1951; Hudson and Fairhurst, 1969). Weibull's distribution describes very well the experimental data obtained for the distribution of heterogeneities in rock. Here we divided the specimen into many finite elements and

assumed that the elemental parameters (failure strength σ_c, elastic modulus E_c, etc.) of rock follow Weibull's distribution law. That is

$$\varphi(\varepsilon_s) = \frac{m}{\varepsilon_0} \left(\frac{\varepsilon_s}{\varepsilon_0}\right)^{m-1} \exp\left[-\left(\frac{\varepsilon_s}{\varepsilon_0}\right)^m\right], \tag{3.1}$$

where ε_s is the element parameter, ε_0 is the mean value of the element parameter and m is the shape parameter. The shape parameter m is defined as the homogeneity index of the rock (Tang et al., 1997; Tang, 1997). A larger m implies a more homogeneous material and vice versa.

According to continuous damage mechanics (Krajicinovic and Silva, 1982), the constitutive law of rock under uniaxial stress conditions can be expressed as

$$\sigma = E\varepsilon(1 - D),$$

where σ and E are the stress and the elastic modulus of the rock specimen, respectively. D is the damage parameter. Based on the heterogeneous material model above, the local strengths are distributed following a Weibull probability distribution. Each element contains unequal numbers of defects and possesses a different strength. As a load is applied, the stress of the local element increases. When the stress satisfies the double elliptic strength criterion (Yu, 1998), the element will fail and be completely damaged. Therefore, the proportion of the locally damaged elements measured in the area is equivalent to the probability that an element fails. The damage parameter D can be represented by the following equation:

$$D = \int_0^\varepsilon \varphi(x)dx. \tag{3.2}$$

Therefore, we can obtain the constitutive law of rock under a uniaxial stress condition as follows:

$$\sigma = E\varepsilon(1 - D) = E\varepsilon\left[1 - \int_0^\varepsilon \varphi(x)dx\right]. \tag{3.3}$$

It is believed that there must be a strong link between the rock damage and the acoustic emission (AE). In other words, the AE activity indicates the extent of local damage in rock, which is directly associated with the evolution and propagation of fracturing within rock. Tang (1997) has derived the following important relationship between the damage parameter D and the AE count N:

$$D = \frac{N}{N_m} = \int_0^\varepsilon \varphi(x)dx. \tag{3.4}$$

By recording the counts of failed elements and released energies when failure occurs, the AE phenomena associated with the progressive failure process can be simulated. Therefore, our elastic damage model not only can represent the irreversible microstructural rearrangement and continuous material degradation that occurs during the failure process, but can also simulate seismicities during the material's continuous damage process.

Based on the interaction of the double rock mass, we simulated numerically the evolution process of the progressive failure leading to sudden fracture by

using the Rock Failure Process Analysis code (RFPA^{2D}). This allowed us to ex-amine the progressive failure process visually on a continuous basis during the loading process.

For the double rock sample model, it was assumed that the two samples have two different Weibull probability density distributions. The rock properties were cho-sen so as to simulate the brittle behavior of rock material. For sample 1, in order to simulate the surrounding body of the rock mass, the mean compressive strength, σ_c was set at 150 MPa; the mean elastic constant E was equal to 65 GPa and Poisson's ratio $\nu = 0.25$. The homogeneity index, m, for the strength was 2 and for the elastic constant, 10. For sample 2, in order to simulate the failed body of the rock mass, the mean strength was set 30% higher. The size of the mesh was 200×200 with 40000 elements to simulate a specimen with a size of 4000 mm $\times$ 4000 mm. The simulation was limited to a two-dimensional problem.

Once the mechanical properties were assigned to the elements, the double speci-men was compressed axially in displacement control mode to simulate a collapse process leading to rockbursts. The total vertical boundary displacement of 30 mm was divided into 100 steps, i.e. 0.3 mm for every step. The samples were loaded in a displacement mode much like the displacement control method in a servo-controlled laboratory test. With a step-by-step increase in external displacement in the axial direction the stress states in some elements may satisfy the strength criterion. Such elements will be damaged and weakened in response to the specified strength criteri-on. The stress and deformation distribution throughout the specimen will be adjusted instantaneously to arrive at the equilibrium state. Due to stress redistribution, the stress state may get to the critical value and lead to further ruptures. The process is repeated until there is no failure rupture element in the sample. Following that, external dis-placement continues to increase. Finally, the system forms macroscopic fractures, releasing the elastic energy stored in the elements as acoustic emissions throughout the onset of element failures during the loading process. Thanks to stress redistribution and long-range interactions, one key element failure may give birth to an avalanche of additional ruptures among adjacent elements, leading to a ripple effect and releasing more energy.

Each increment of the displacement is regarded as a disturbance induced by mining. The numerical simulation is the same as for the elastic finite element method. When the twin sample is loaded step by step, the positions of the elements change, and so do the stresses and strains of the elements.

3.1 Progressive Failure Leading to the Collapse of a Single Pillar

When the applied boundary displacement increases, Fig. 5 shows the progressive failure process obtained in the simulation. The relative stress distribution, stress-strain and AE plots presented in Fig. 5 were calculated using the following equation:

$$\frac{\sigma_s}{\sigma_c} = \frac{\sigma_1}{\sigma_c} - S\frac{\sigma_3}{\sigma_c}, \tag{3.5}$$

where σ_s/σ_c represents the severity of an element or its proximity to failure. The brightness of the gray shading in the plots indicates the stress levels (high = white,
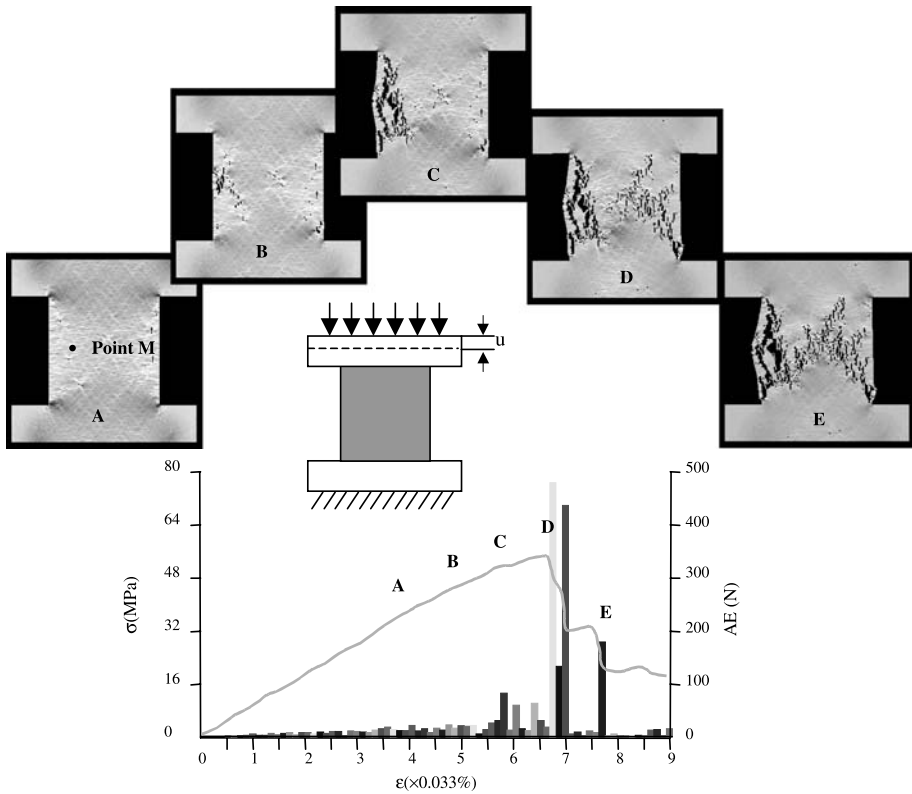
Fig. 5. Numerically-simulated pillar failure process and the corresponding plots of stress-strain and strain-AE

low = black). The following stages were observed during the progressive failure process:

1) During the initial loading phase (low stress level), a few fractures are localized and relatively sparse, with only a few seismic events occurring. The stress-strain behavior is nearly elastic during this stage (Stage A in Fig. 5). Therefore, this state corresponds to the stable pillar deformation stage.

2) Then, a population of randomly located, non-interacting fractures is observed in the left side of the pillar. Due to the heterogeneity of rock, the distribution of fractures is not symmetrical; a few fractures occur only in the right foot of the pillar. These sequences involve a limited number of isolated fractures because of the side distribution of weak elements. The principal characteristic of this stage of deformation is diffuse, heterogeneous microfracturing of the entire rock mass. The stress-strain curve becomes non-linear in this stage (stage B in Fig. 5), and this stage is named the sub-stable pillar deformation stage.

3) As microfracture damage accumulates, fractures become clustered, involving more elements, leading to fracture interaction and development in the left side of the pillar. As more damage accumulates, large clusters emerge before main fracture
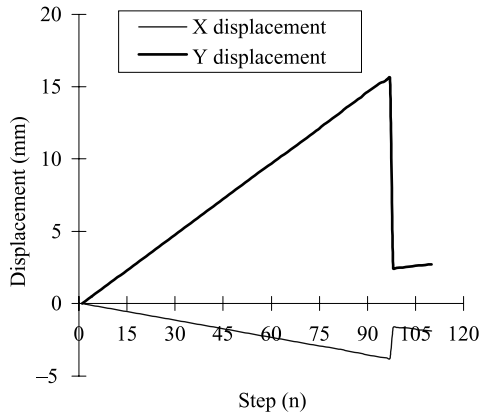
Fig. 6. A sudden displacement drop at Point *M* of the pillar with the load increasing

nucleation. Meanwhile, the corresponding acoustic emission is evident. The stress-strain curve shows strain-weakening behavior, with a small stress drop (stage C in Fig. 6). Accordingly, this stage is attributed to an unstable pillar forewarning stage.

4) Eventually the number of failed elements increases drastically, mainly concentrating in the right area of the pillar, and clusters gradually in the central area. The pillar becomes mechanically unstable, i.e. the elements in the weaker zone suddenly collapse, forming a fault. At this time two large stress drops occur, which can be seen in stage *D*, while the corresponding acoustic events are 5 times those in stage *C*. This semi-static model does not enable the simulation of the dynamic shoot-off of rock, so many micro-fractures occurring abruptly and the drastic stress drop can be regarded as the apparent feature of pillar rockburst. Furthermore, it is clear from Fig. 6 that there exists a sudden drop of displacement in this stage, which also demonstrates that this stage is the unstable pillar failure stage (Stage *D* in Fig. 5).

5) The stress field of the fault concentrates around it, producing further micro-fracture damage around and ahead of its tips. This stress concentration leads to another new clustering of micro-fractures occurring at point *E*. However, both the stress drop and the acoustic emission events are not stronger than those in point *D*. Nevertheless, a macro shear fault is formed in this stage. Although the post micro-fractures become fewer and fewer, the pillar retains a certain bearing capability. Therefore this stage is called the residual pillar deformation (Stage *E* in Fig. 5).

It is worth noting that in Fig. 6 a sudden displacement jump occurs at point *M* during the loading process. The maximum Y-displacement jump is 14 mm, while the X-displacement jump is 3 mm, which is in agreement with the cusp-type catastrophe model discussed above.

3.2 Rock Mass Reponse Test

Two single pillar models were constructed to investigate the effect of the loading system stiffness on the failure mode and the induced seismic pattern in the rock mass.

Table 1. Material parameters for tests of stiffness effects

		Model I	Model II
Elasticity parameter	roof and floor	300 GPa	30 GPa
	pillar	60 GPa	60 GPa
Strength parameter	roof and floor	200 MPa	200 MPa
	pillar	200 MPa	200 MPa
Poisson's ratio	roof, floor and pillar	0.25	0.25
Homogeneity index	Elasticity	20	20
	Strength	3	3

The pillar and host rock strength were the same in both models, but the rock mass in the pillar was assumed to be relatively heterogeneous in terms of strength (Table 1; m = 3). In model I, the roof and floor rocks were five times stiffer than the pillar, whereas in model II, the elastic modulus for the roof and floor was half of the pillar modulus, to simulate a soft loading condition. The material parameters used in the models are summarized in Table 1.

The two-dimensional mesh for each model consisted of 320×100 elements to simulate a specimen with a size of 3200 mm $\times$ 1000 mm and the models were loaded vertically in a displacement control mode. The total vertical boundary displacement of 50 mm was divided into 100 steps, i.e. 0.5 mm for every step.

Figures 7a–c and 8a–c show (a) the failure mode development with the vertical displacement increasing, (b) the associated seismic source locations, and (c) the stress, strain and acoustic emission records for pillars under a progressively increasing vertical boundary displacement.

In the pillar with a stiff host rock (roof and floor), pre-peak nonlinearity was caused by a dispersed microfracturing pattern (Fig. 7b, 0–0.55u) until a distinct shear plane formed (0.56u) leading to the first strength drop at peak strength (Fig. 7c). The shear plane was inclined at 53–63° to the loading axis (Fig. 7a and b). Fig. 7a shows that the heterogeneity of the sample caused the formation of a relatively flat shear nucleation zone (0.55u) in the center of the sample. This was preceded by the development of localized seismic activity centers, causing a rock mass damage cluster (0.50u–0.53u) due to the pillar's heterogeneous strength. Moreover, new shear planes occurred parallel to the former one, and some clustering fractures were formed between the two parallel shear planes (Fig. 7a, 0.62u–0.77u). The highest number of seismic emissions and most released energy were observed during the first stress drop when the shear zone formed (0.56u). Several additional stress drops in the post-peak range (between 0.21 and 0.35% strain) were observed (Fig. 7c) when the shear zone was extended to the pillar boundary (0.61u–0.69u). Each stress drop was associated with an elevated emission count and elevated energy release rate (Fig. 7c).

When loaded with a soft host rock ($E_{host} = 0.5E_{pillar}$) with the same Poisson's ratio (Fig. 8a and c), the first shear fractures (e.g. 0.53u), and the ultimate shear planes at the end of the failure process, formed almost in the diagonal direction (Fig. 7a). It is necessary to note that the pre-peak stress-strain curves were almost identical (Figs. 7c and 8c) for the two models. However, as expected, the rock loaded in a softer system exhibited a more brittle post-peak failure pattern with a sharper post-peak slope.
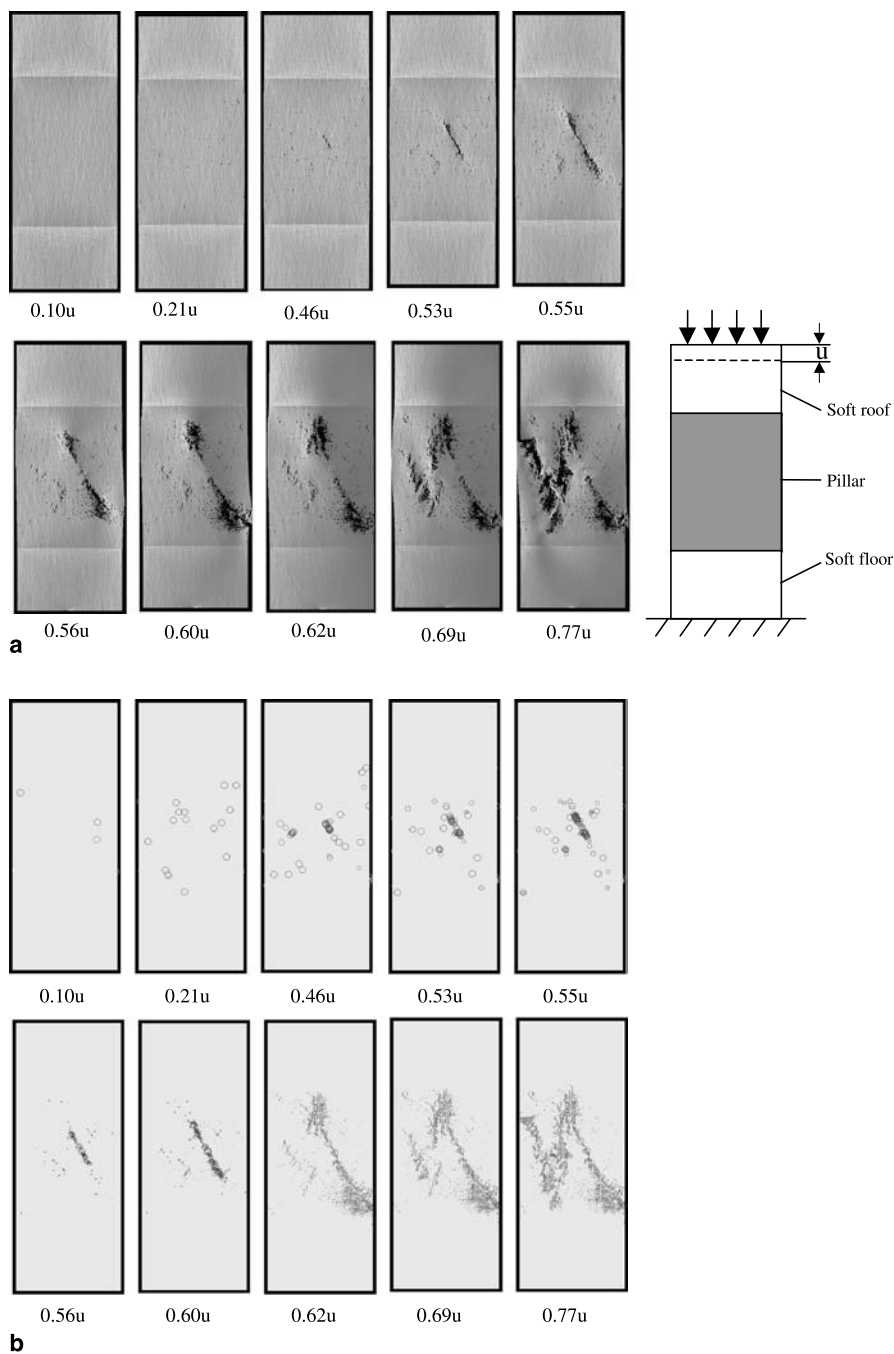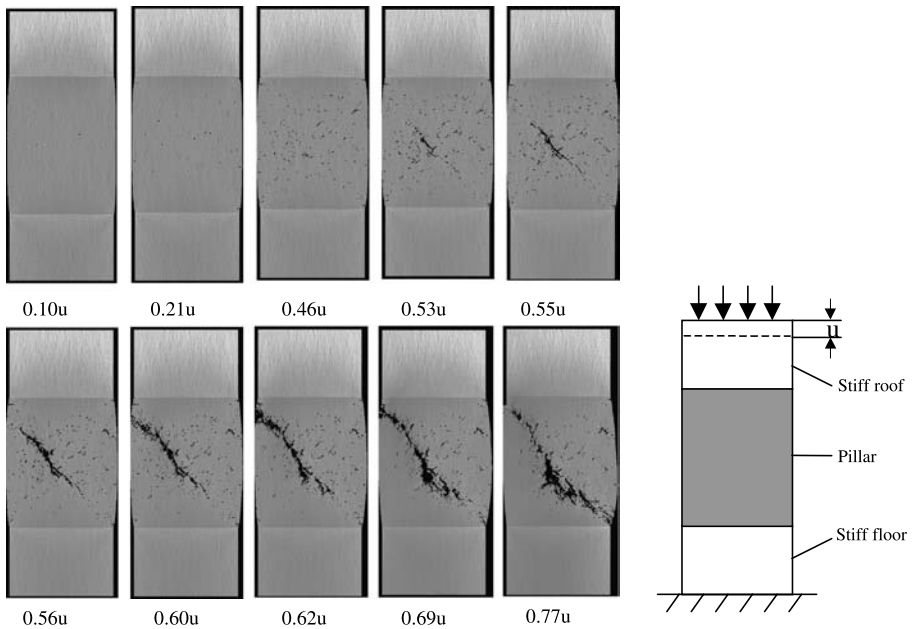
Fig. 7. a Maximum shear stress distribution with soft host rock (roof and floor). **b** Seismic source location with stiff host rock (roof and floor)
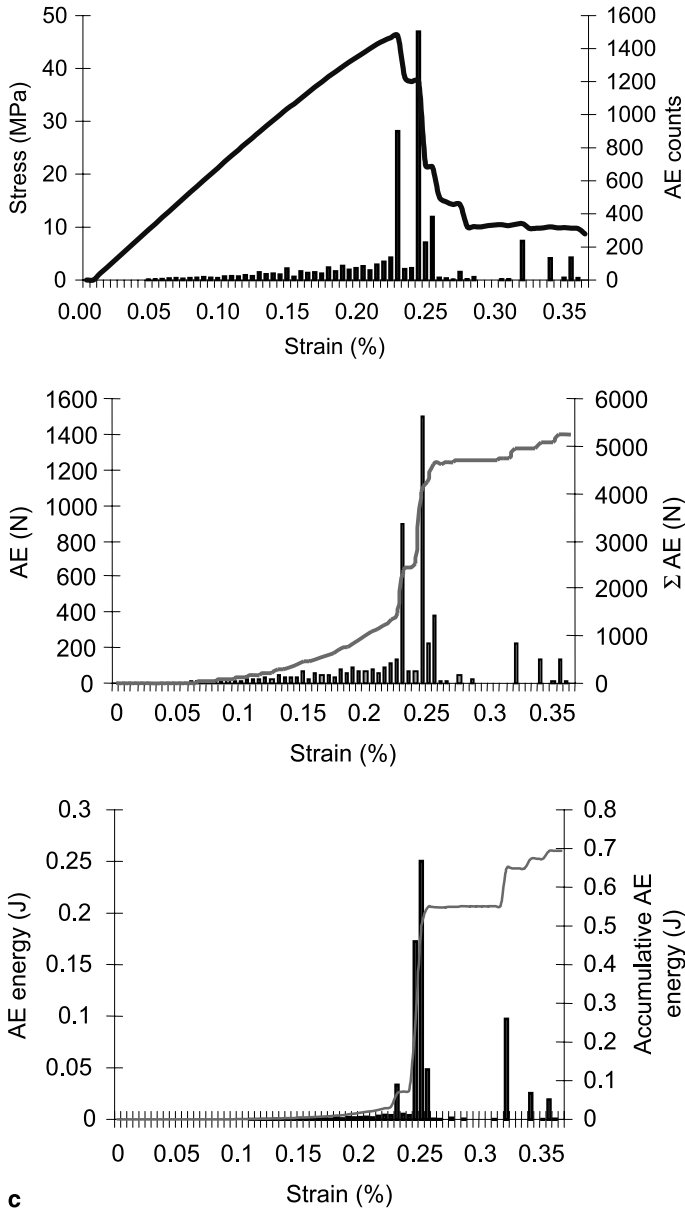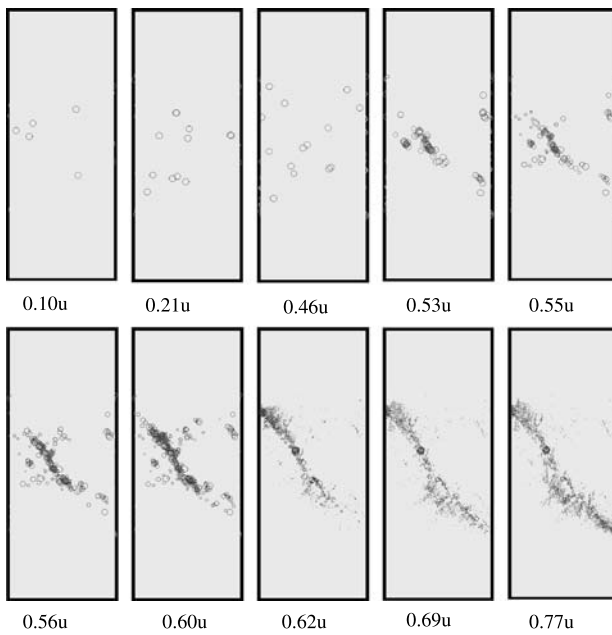
Fig. 7c. Stress-strain, seismic event and seismic energy release with stiff host rock

Although the concentrations of seismicity in the soft loading condition were fewer than that in the stiff loading condition ($N_{max} = 1560$ vs. 1080 at 0.55u and 0.56u, respectively, when the through-going shear zone formed), almost two times as much energy was released at this loading step (0.48 vs 0.26 at 0.55u). This indicates that soft loading conditions can induce more dangerous failures.
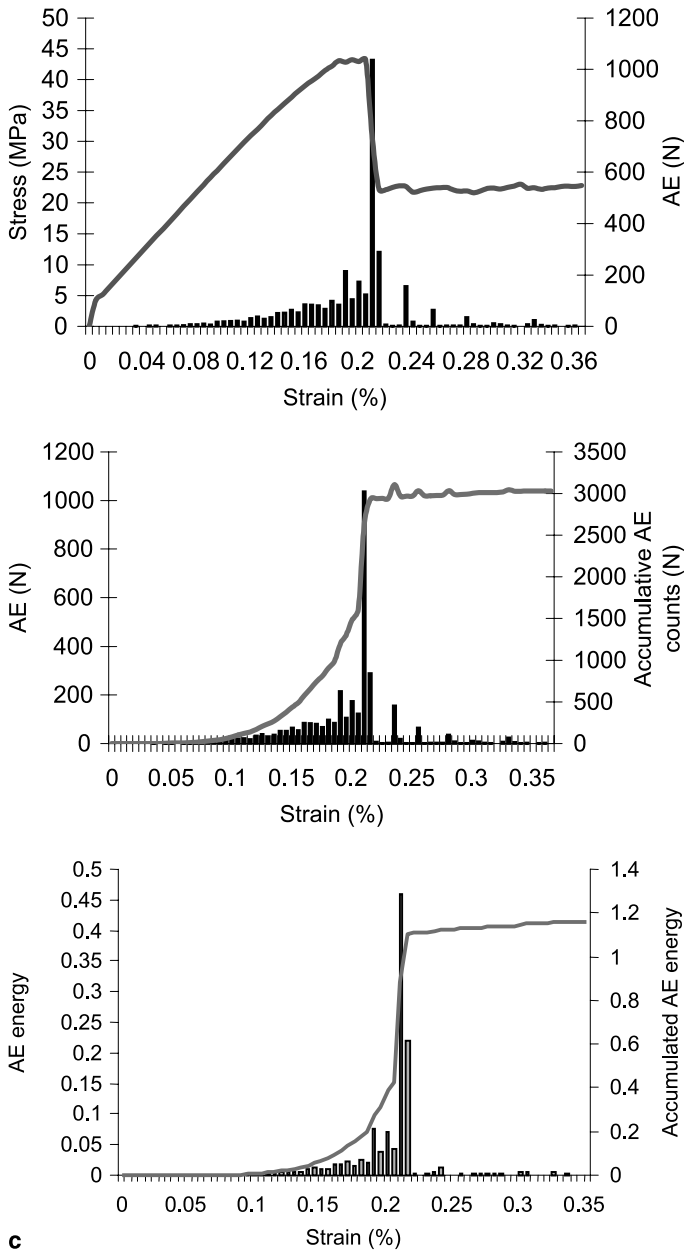
Fig. 8. a Maximum shear stress distribution with soft host rock (roof and floor). **b** Seismic source location with soft host rock (roof and floor)

Fig. 8c. Stress-strain, seismic event and seismic energy release with soft host rock

In both cases, seismic emissions started at approximately one third of peak strength (at the crack initiation level (Martin and Chandler, 1994) whereas noticeable energy release was only observed at around 80% of the peak strength, i.e. when the stress-strain curve deviated from an initial linearity, the internal energy release asso-

ciated with each event caused stress redistribution within the rock sample and this, in turn, eventually led to failure propagation by shear-zone formation. Initially, this stress redistribution process was dispersed, causing little deviation from linearity. When nucleation zones or damage clusters developed, the overall response became non-linear. Eventually, when the energy release was concentrated (Fig. 8c), as driven by the soft loading system, the shear zone formed almost instantaneously and the post-peak slope of the stress-strain curve was very steep. Post-peak energy release peaks were observed when ''rock bridges'' failed as indicated by various seismicity clusters (0.57u–0.69u; Fig. 7b). The AE count recorded before the peak varied little between the two models (45–47% of all recorded events). However, 30% of the AE counts were recorded during the shear-zone formation in the soft-loading system, as compared to only 16% with the stiff host rock. As a consequence, fewer AE counts were recorded after the main event in the soft loading system (23 vs. 39%). This suggests that prolonged seismic activity may be an indicator of a relatively stiff loading environment.

With respect to energy release, 75% more energy was released from the pillar with a soft host rock for the chosen model parameters. 16 and 18% were released before the peak, and 28 and 42% at the peak for the stiff and soft system, respectively. The energy stored in the softer loading system drove the failure process and caused the higher energy release during the shear-zone formation process. This left 39 and 22% of the energy release for ''aftershocks'' in the stiff and soft system, respectively. However, in absolute terms, the total post-peak energy release was equal for the two models because the soft system released 75% more energy, as indicated above.

Jaeger and Cook (1969) pointed out that, in a relatively stiff environment, the dilation process of the failing rock is controlled and the rock mass strength is lost gradually. Conversely, in soft mine settings, rock mass dilation is driven by energy release from the surrounding rock mass which leads to rapid and violent failure, possibly with rock ejection. The two models presented here illustrate and quantify this process.

4. Summary and Conclusions

In this paper, a simple mechanical model was proposed for unstable rock failure under the action of a loading system, and the mechanism of instability was studied using a cusp-type catastrophe model. It was shown theoretically that the stiffness ratio, K, of the machine to the specimen plays an important role in the outbreak of instability. Simple formulae for the deformation jump and the energy release were derived. The outcome of the research shows clearly that the stability characteristic of the rock–rock (hypocenter surrounding rock) system is determined by the stiffness distribution in the system and that the condition for instability is $K > 1$.

The physical process resulting in a rockburst is a damage evolution process stemming from microseismic development to a sudden main shock owing to an interaction between the two parts of the rock mass. The spatial distribution of microseismic events prior to the main shock is transformed into a distribution along a narrow zone. Based on the assumption that each failed element can contribute an increment of

microseismicity, a simple statistical model was introduced and the qualitative micro-seismic rate of the double rock sample was obtained.

By using the RFPA code, the interdependence of stress, strain, acoustic or seismic emissions, and seismic energy release was illustrated, and the evolution process of microseismic activity and its spatial distribution were simulated during the rock pillar failure process. Research results have been given in this paper, which indicate that using the RFPA code it is possible to predict the occurrence of rockbursts when a sudden decrease in the microseismic rate occurs in one zone while the microseismic rate continues to increase in an adjacent zone. The numeri-cally simulated results are in fairly good agreement with the theoretical considera-tions proposed and thus verify the reliability of catastrophe theory as applied to the study of rock.

Acknowledgements

References

Cook, N. G. W. (1976): Seismicity associated with mining. Eng. Geol. 10, 99–122.

Cubiu, J., Shaw, B. (1976): The geological implications of steady-state mechanisms in Catas-trophe Theory. Math. Geol. 8, 657–661.

Gill, D. E., Abortion, M., Simon, R. A. (1993): Practical engineering approach to the evaluation of rockburst potential. In: Young, R. P. (ed.), Rockbursts and seismicity in mines. pp. 63–68.

Henley, S. (1976): Catastrophe Theory Model in geology. Math. Geol. 8, 649–655.

Hudson, J. A., Fairhurst C. (1969): Tensile strength, Weibull's theory and a general statistical approach to rock failure. In: Proc., Civil Engineering Materials Conference, Southampton, pp. 901–904.

Jaeger, J. C., Cook, N. G. W. (1969): Fundamentals of Rock Mechanics. Methuen, London.

Krajcinovic, D., Sumarac, D. (1989): A mesomechanic model for brittle deformation processes, Part I. J. Appl. Mech. 56, 51–62.

Krajicinovic, D., Silva, M. A. G. (1982): Statistical aspects of the continuous damage theory. Int. J. Solids Struct. 18, 551–562.

Lockner, D. A., Madden, T. R. (1991): A multiple-crack model of brittle fracture. J. Geophys. Res. 96(19), 623–19, 642.

Lockner, D. A., Moore, D. E., Reches, Z. E. (1992): Microcrack interaction leading to shear fracture. In: Tillerson, J. R., Wawersik, W. R. (eds) Proc., 33rd Symposium on Rock mechanics, Balkema, Rotterdam, pp. 807–815.

Martin, C. D., Chandler, N. A. (1994): The progressive fracture of Lac du Bonnet granite. Int. J. Rock Mech. Min. Sci. 31(6), 643–659.

Rice, J. R. (1983): Constitutive relation for fault slip and earthquake instability. Pageoph 121, 443–475.

Salamon, M. D. G. (1993): Some application of geomechanical modeling in rockburst and related research. In: Young, R. P. (ed.), Rockbursts and seismicity in mines. 297–309.

Saunders, P. T. (1980): An introduction to Catastrophe Theory. Cambridge University Press, Cambridge.

Tang, C. A. (1993): Catastrophe in rock unstable failure (in Chinese). China Coal Industry Publishing House, Beijing, 26–27.

Tang, C. A. (1997): Numerical simulation of progressive rock failure and associated seismicity. Int. J. Rock Mech. Min. Sci. 34, 249–262.

Tang, C. A, Hudson, J. A., Xu, X. H. (1993): Rock failure instability and related aspects of earthquake mechanisms. China Coal Industry, Beijing.

Tang, C. A., Chen, Z. H., Xu, X. H., Li, C. (1997): A theoretical model of the Kaiser effect in rock. Pure Appl. Geophys. 150, 203–215.

Weibull, W. (1951): A statistical distribution function of wide applicability. J. Appl. Mech. 293–297.

Yin, Y.-Q., Zheng, G.-T. (1988): A cusp-type catastrophic model of fault earthquakes, Acta Geophys. Sin. 31(6) 657–663.

Yu, M. H. (1998): Double twin strength criterion and its application. Science Press, Beijing, (in Chinese).

Author's address: Dr. Shanyong Wang, Department of Building and Construction, City University of Hong Kong, Tat Chee Avenue 83, Kowloon, Hong Kong; e-mail: bcwangsy@cityu.edu.hk